Journal of Power Sources 522 (2022) 230986

Contents lists available at ScienceDirect

Journal of Power Sources

journal homepage: www.elsevier.com/locate/jpowsour

Impedance spectroscopy study of Au electrodes on Gd-doped CeO_2 (GDC) – Molten Li_2CO_3+Na_2CO_3 (LNC) composite electrolytes

Vijayan Sobhana Dilimon, Ragnar Strandbakke, Truls Norby *

Department of Chemistry, University of Oslo, FERMiO, Gaustadalléen 21, NO-0349 Oslo, Norway

HIGHLIGHTS

- No interface contribution to ionic conduction in molten carbonate GDC composites.
- GDC is catalytic to Au electrode in molten carbonate in O_2, but not in presence of CO_2.
- CO_2 adsorbs on and blocks GDC surfaces, but not $LiAlO_2$ surfaces.
- No benefit of GDC composite over traditional MCFC $LiAlO_2$ composite and NiO cathode.
- Two-step O_2 reduction and mass transport by peroxide (in O_2) or oxycarbonate (in CO_2).

ARTICLE INFO

Keywords:
Molten carbonate fuel cells
MCFC
CeO_2
Gd-doped
GDC
GDC-Molten carbonate composite electrolyte
Oxygen electrode
Mechanism

ABSTRACT

We herein report an impedance spectroscopy study of Au electrodes on Gd-doped CeO_2 (GDC) – molten Li_2CO_3+Na_2CO_3 (LNC) composite electrolytes in O_2 and O_2+CO_2 atmospheres. Complementary measurements of Au on GDC alone are provided for supporting insight. We find that the adsorption of CO_2 on GDC in O_2+CO_2 atmospheres effectively blocks oxygen adsorption and severely slows oxygen reduction kinetics. The conductivity of the composite is dominated by the GDC phase in the solid-solid temperature region, while the LNC phase dominates above its melting point, and no further enhancement e.g. by interfacial effects are found. The incorporation of LNC melt into GDC results in a significant reduction in the polarisation resistance of Au electrodes in O_2 atmospheres, as the melt mediates the reaction by a peroxide mechanism. In O_2+CO_2 atmospheres, however, the polarisation resistance of Au electrodes on GDC-LNC membranes is significantly higher, higher even than that on GDC. This we assign again to the blocking adsorption of CO_2 (or carbonate) on the surfaces of ceria and the sluggish transport and reactions now mediated by carbonate-carried oxide species (CO_4^{2-}) instead of peroxide species.

1. Introduction

Composite electrolytes comprising an oxide ion conducting doped ceria frame impregnated with a mixture of alkaline carbonates show conductivities above 0.1 S cm^{-1} at 600 °C and are suggested candidates for what is referred to as molten carbonate fuel cells (MCFCs) or intermediate temperature solid oxide fuel cells (ITSOFCs) [1,2].

In MCFCs, the cathode side is fed with a mixture of O_2 and CO_2 and the oxide ions (O^{2-}) formed in the cathodic reaction combine with CO_2 to form carbonate ions, which migrate to the anode side [3]. At the anode side, the oxidation of fuel (say H_2) to H_2O occurs by means of the carbonate ions, with regeneration and need for recycling of CO_2.

The molten carbonate phase supports conductivity by carbonate ions and alkali metal ions, with minor additional contributions from other ionic species like oxide and hydroxide ions dissolved in equilibrium with O_2 and H_2O in the gas phase. The introduction of oxide ion conductors like GDC instead of the traditional $LiAlO_2$ ceramic phase aims to increase the oxide ion conductivity to increase the overall electrolyte conductivity, to speed up electrode kinetics, or achieve mixed carbonate and oxide ion conductivity for use in CO_2-permeable membranes. In addition to transport in the oxide phase and the molten phase, some researchers have proposed enhanced transport, including the existence of highly conducting space-charge layers ("superionic highways") at the solid oxide - molten carbonate interface, embraced in many publications to

* Corresponding author.
E-mail address: truls.norby@kjemi.uio.no (T. Norby).

https://doi.org/10.1016/j.jpowsour.2022.230986
Received 2 November 2021; Received in revised form 3 January 2022; Accepted 6 January 2022
Available online 13 January 2022

justify the high conductivity of solid oxide - molten carbonate composite electrolytes [4–9]. Other studies, however, have shown similar conductivities for CeO_2-LNC and GDC-LNC as for $LiAlO_2$-LNC (LNC = Li_2CO_3/Na_2CO_3 eutectic) [10,11], Discrepancies may to some extent be ascribed to the neglect of the instability of the carbonate phase in CO_2-free atmospheres.

The complexity of the reduction of O_2 at the cathode generally determines the overall performance of MCFCs and "ITSOFCs" based on molten carbonate composites [12–15]. Still, electrode reactions on composite electrolytes comprising oxide ion conducting ceramics and molten carbonate have so far not been studied experimentally in a systematic fashion.

The molten carbonate phase has been shown to facilitate the cathodic oxygen reduction reaction (ORR) when present in $La_{0.8}Sr_{0.2}MnO_{3+\delta}$+$Ce_{0.8}Gd_{0.2}O_{2-\delta}$ (LSM + GDC) [16] and $La_{0.6}Sr_{0.4}Fe_{0.8}Co_{0.2}O_{3-\delta}$+$Gd_{0.2}Ce_{0.8}O_{1.9}$ (LSCF + GDC) [17] composite cathodes in CO_2-free atmospheres. It was suggested that this relies on fast oxygen transport through the molten carbonate phase by a cooperative "cogwheel" (or "paddle wheel") type mechanism of oxygen atoms forming CO_4^{2-} species with – and jumping between – CO_3^{2-} ions. Computational studies support the thermodynamic stability of CO_4^{2-} in CO_2-free atmosphere and the cooperative 'cogwheel' type O transfer in oxide-carbonate composite electrolytes [4,18,19]. One of these studies suggested that the O cogwheel transport in yttria-stabilized zirconia (YSZ) – Li_2CO_3+K_2CO_3 composites could be faster through the oxide-carbonate interphase than through the bulk carbonate phase [4]. However, Chen et al. [20] showed by in situ Raman spectroscopy that peroxide (O_2^{2-}) is the only stable oxygen species in Li_2CO_3+K_2CO_3 melts in CO_2-free atmospheres. In O_2+CO_2 atmospheres, however, only CO_4^{2-} or $C_2O_6^{2-}$ species were identified, no peroxide [21]. Following the spectroscopic results of Chen et al. and seeing that CO_4^{2-} and $C_2O_6^{2-}$ are not present in CO_2-free atmosphere, the lower polarisation resistance (R_p) for ORR when molten carbonate is added to LSM + GDC or LSCF + GDC cathodes must be explained by peroxides – and not CO_4^{2-} – as the active oxygen species.

The present work is to our knowledge the first attempt of an experimental study of the electrode kinetics and mechanism on oxide-molten carbonate composite membranes. We use gold (Au) as a model electron conductor, and compare its behavior on GDC-LNC composite membranes with that on simple GDC and composite $LiAlO_2$-LNC membranes.

2. Experimental methods

2.1. Preparation of composite membrane

GDC nanopowder ($Ce_{0.8}Gd_{0.2}O_{2-\delta}$, Sigma Aldrich, <100 nm) was coarsened at 1500 °C for 1 h. The coarsened powder was ground with a binder (20 drops g^{-1}) in a mortar into a fine powder. The binder used was 5 wt% PARALOID B-60 + 5 wt% PARALOID B-72 + 90 wt% ethyl acetate. The powder was pressed into disks (20 mm diameter and 2.5 mm thickness) at a force of 7 tons for 3 min. The pellets were then sintered at 1500 °C for 4 h, to a relative density of 70 ± 2%. A mixture of Na_2CO_3 (Sigma Aldrich) and Li_2CO_3 (Sigma Aldrich) in the eutectic composition (48:52 M ratio) was melted in an alumina crucible at 700 °C by using a split vertical tube furnace. The sintered GDC pellet, suspended at the end of a platinum wire, was preheated just above the crucible with the molten carbonate eutectic for 30 min and then dipped into and fully immersed in the melt for 90 min. The impregnated pellet was pulled out of the melt and further out through the column of the furnace very slowly to avoid pellet breakage. The composition of pellets was typically ~70 vol%, GDC, ~30 vol% LNC, and <3 vol% porosity.

Precursors for the preparation of $LiAlO_2$-LNC composite membranes ($LiAlO_2$ (Sigma Aldrich), Na_2CO_3 (Sigma Aldrich), and Li_2CO_3 (Sigma Aldrich)) were mixed ~70 vol% $LiAlO_2$ and ~30 vol% LNC and finely grinded by using mortar and pestle. The powder was pressed into disks (20 mm diameter and 2.5 mm thickness) at a pressure of 7 tons for 3 min. The GDC-LNC and $LiAlO_2$-LNC pellets were finally polished with a fine emery paper.

2.2. Electrochemical studies

The composite pellets were painted with gold paste (1 cm^2) on both sides, dried at 120 °C in air, and sintered in air for 1 h at 600 °C. The pellets were contacted with Pt current collectors in a 2-point, 4-wire configuration and mounted in a ProboStat™ sample holder cell (NORECS, Norway) with alumina support tube. Gas mixtures similar to the ones described in the literature were used to control the atmosphere in the cell [22]. The GasMix program 0.7.1 (NORECS, Norway) was used to calculate the flowmeter levels required to generate a particular gas composition.

EIS was done on the symmetrical cells at open circuit potential by a Solartron SI 1260 Impedance/Gain-phase analyzer at 1 MHz - 0.01 Hz with an oscillation voltage of 50 mV RMS. Impedances for Nyquist plots and derived electrode polarisation parameters are obtained by division by 2 and taking the electrode area into account to obtain area specific parameters per electrode. The impedance data were fitted by using the Zview software (Scribner Associates Inc.).

3. Results and discussion

3.1. Electrolyte conductivity

Fig. 1 compares the impedance spectra in O_2 and O_2+CO_2 atmospheres of Au electrodes on GDC, GDC-LNC, and $LiAlO_2$-LNC membranes at 600 °C. The electrolyte resistances – obtained from the high-frequency intercept with the real axis – are much lower for the solid GDC-molten carbonate composites than for the solid GDC membrane, showing that the molten carbonate phase dominates the electrolyte conductivity. GDC-LNC and $LiAlO_2$-LNC composite membranes have the same electrolyte conductivity within experimental error at this and all other temperatures investigated, showing that there is no significant contribution from interfacial conduction between the GDC and the molten carbonate, in contradiction to claims in certain literature [8].

3.2. Membranes influence R_p differently in O_2 and O_2+CO_2 atmospheres

Fig. 1A shows that the overall R_p of Au electrodes on the molten carbonate impregnated membranes in O_2 atmospheres are significantly lower than that of Au on unimpregnated GDC membranes. It agrees with reports [16,17] showing a catalytic effect of molten carbonates for the ORR. The overall R_p of Au on GDC-LNC and $LiAlO_2$-LNC composite membranes in O_2 atmospheres were comparable. This shows that the solid oxide phase does not influence the electrode reaction on these membranes in O_2 atmospheres, and that the molten carbonate phase alone is responsible for the enhanced ORR rate.

Fig. 1B shows that the trend of R_p in O_2+CO_2 atmospheres is entirely different from that in O_2 atmospheres. The R_p values of Au on oxide-carbonate membranes are now higher than that on the GDC membrane, which in turn is increased from CO_2-free atmosphere despite increased partial pressure of O_2 (p_{O_2}) in O_2+CO_2 atmospheres. Interestingly, the GDC-LNC membrane, which has an oxide ion conducting ceramic phase, shows significantly higher R_p than $LiAlO_2$-LNC. Thus, GDC inhibits – or $LiAlO_2$ promotes – the electrode reaction involving CO_2. As CO_2 in the feed gas to the cathode side of MCFCs is indispensable, these observations suggest that GDC as the solid phase in molten carbonate membranes has no advantage for MCFCs.

The Raman spectroscopic studies by Chen et al. showed peroxide and CO_4^{2-} as the oxygen species formed in the melt in O_2 and O_2+CO_2 atmospheres, respectively [20,21]. The ORR by peroxides (CO_2-free atmosphere) can therefore as a first approximation be seen as faster than the ORR by CO_4^{2-} (O_2+CO_2 atmosphere).

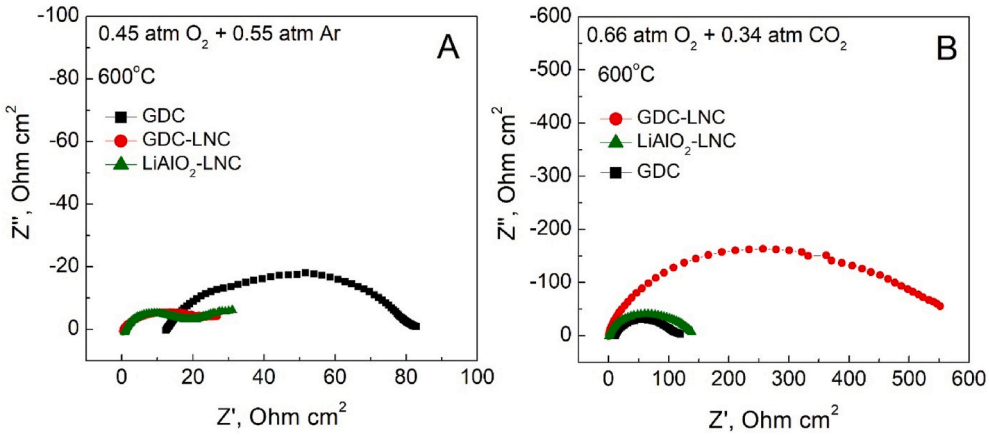

Fig. 1. Impedance spectra of the Au electrode on GDC, GDC-LNC, and $LiAlO_2$-LNC membranes at 600 °C. A: O_2 atmosphere, B: O_2+CO_2 atmosphere.

3.3. GDC interacts with CO_2

Fig. 2 compares the electrode impedance behavior of the Au electrode on the solid GDC electrolyte in O_2 and O_2+CO_2 atmospheres at 625 °C. The overall R_p on the GDC membrane is significantly higher in O_2+CO_2 atmospheres than in O_2 atmospheres. While basic (electron-rich) gas molecules react with the acidic surface cation sites of CeO_2, acidic (electron-poor) molecules such as CO_2 react with surface O^{2-} sites, forming carbonate species according to DFT calculations and experimental studies [23–27]. Such strong adsorption and desorption of CO_2 on CeO_2 at low and high temperatures have suggested use of CeO_2 for CO_2 capture from emission sources [28,29]. Moreover, the adsorbed CO_2 in a bent anionic configuration is in an activated state facilitating subsequent reactions such as CO_2 dissociation [25].

Fig. 2 (inset A & B) shows a sharp increase in the overall R_p when CO_2 is added to Ar in the gas mixture. We conclude from this that the CO_2/CO redox reaction is slow on the Au-GDC electrode (does not contribute) and that CO_2 adsorbs and blocks the O_2/O^{2-} redox reaction, which is believed to occur by traces of oxygen in the Ar/CO_2 atmosphere. At 625 °C, the high overall R_p does not show any variation with increasing the partial pressure of CO_2 (p_{CO_2}) from 0.37 to 0.77 atm, indicating a saturation of adsorbed CO_2 (Fig. 2 (inset A)), in agreement with ambient pressure XPS studies of CO_2 adsorption at 500 °C by Feng et al. [30], while the overall R_p increased with increasing p_{CO_2} at higher temperatures (Fig. 2 (inset B)), in line with partial CO_2 coverage.

3.4. Au on GDC in O_2 atmosphere

Fig. 3 shows the electrode impedance behavior of Au on the GDC membrane in CO_2-free Ar + O_2 atmospheres. The overall R_p decreases with increasing p_{O_2}. Fig. 3 (inset) shows the equivalent circuit used for the impedance data fitting, comprising the ohmic resistance R_b, and parasitic inductance, L. The high-frequency polarisation resistance R_{hf} can be related to charge transfer at the electrode/electrolyte interface, coupled over the double layer capacitance (modelled with a constant phase element CPE1 with characteristic area-specific capacitances around 4×10^{-6} F cm^{-2}). The low-frequency polarisation resistance R_{lf} is coupled over a chemical capacitance (CPE2, around 2×10^{-2} F cm^{-2}) and can be associated with a mass transfer process, such as reaction kinetics [31]. Gas diffusion impedance is not anticipated to play a role based on 1) the moderate capacitance, 2) the Au electrode had a coarse microstructure and the GDC was sintered and coarsened at 1500 °C still with 30% open porosity, 3) the gas compositions are not very dilute, and 4) oscillation voltages are limited to 50 mV rms.

A theoretical discussion of reaction models for the oxygen reduction at the Au,O_2(g)/YSZ interface shows that mixed control by charge and mass transfer results in a second capacitive response (arc) in addition to

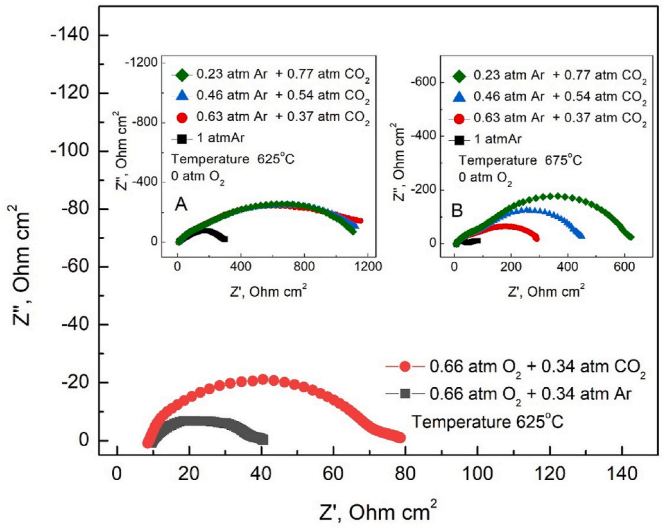

Fig. 2. Complex impedance of the Au electrode on GDC in O_2 and O_2+CO_2 atmospheres at 625 °C. Insets show the electrode reaction impedance under different p_{CO_2} at A: 625 °C and B: 675 °C.

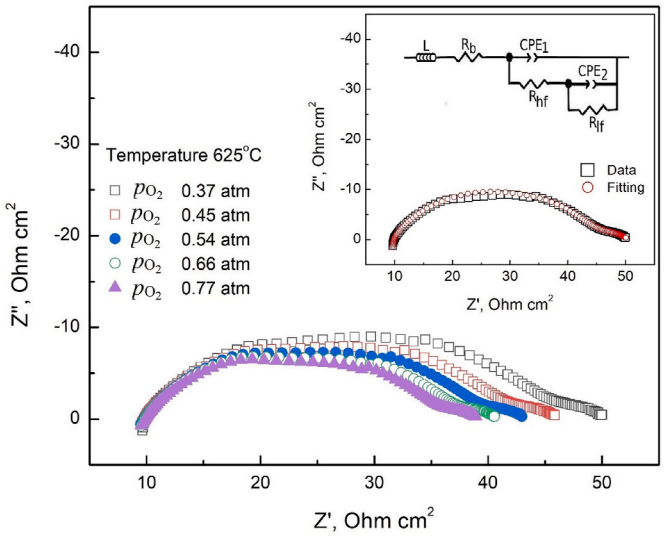

Fig. 3. The electrode reaction impedance of Au on GDC at 625 °C in Ar + O_2 with different p_{O_2}. Inset: Equivalent circuit and fitted spectrum.

that related to charge transfer in parallel with the double layer capacitance [32], like we see in the impedance spectra in Fig. 3. Arrhenius plots (Fig. 4A) show that the reaction step corresponding to the charge transfer high-frequency arc has an activation energy of around 1.37 eV, while the mass transfer low-frequency arc has an activation energy of around 1.06 eV.

The overall ORR occurring at the interface of an electrode and an oxide ion conducting electrolyte can be represented as

$$O_2(g) + 4e^- + 2v_o^0 \rightarrow 2O_o^{2-} \quad (1)$$

where v_o^0 and O_o^{2-}, respectively, represent oxygen vacancies and oxide ions in the electrolyte. This overall reaction can involve a series of consecutive steps, each of which can be the rate-determining step (rds). The overall ORR is made up of two essential parts. The first part represented as $O_2(g) \rightarrow 2(O_{ad(CTS)})$ includes the reaction steps bringing oxygen to the charge transfer site (CTS). The second part includes charge transfer steps, and can be represented as $O_{ad(CTS)} + 2e^- + V_o^0 \rightarrow O_{o(GDC)}^{2-}$. The current ($i$) – overpotential ($\eta$) relationship takes the form of the Butler-Volmer relation [33].

$$i = i_0[\exp(\alpha_a f\eta) - \exp(-\alpha_c f\eta)] \quad (2)$$

where i_0 is exchange current density, α_a and α_c anodic and cathodic charge transfer coefficients, and $f = F/RT$ (F Faraday constant, R gas constant, T absolute temperature). We can get information about the sequence of elementary steps and the type of species involved in the rds from the n-value in relation 3 that expresses the dependence of i_0 (from equation (2)) on p_{O_2}. For small overpotentials, the exchange current density (i_0) is inversely proportional to R_p, so,

$$i_0 \propto \frac{1}{R_P} \propto p_{O_2}^n \quad (3)$$

The polarisation study by Wang and Nowick of Au electrodes on doped ceria electrolytes showed an n-value of 3/8 with $\alpha_a = \frac{3}{2}$ and $\alpha_c = \frac{1}{2}$ [34]. They explained it by proposing an ORR mechanism that involves diffusion of atomic oxygen along the two-phase electrode/electrolyte contact followed by charge transfer as the rate-limiting process. A similar explanation has been given for the n-value of 3/8 for Pt on doped ceria electrolytes [35].

Fig. 4B shows the dependence of $1/R_{lf}$ and $1/R_{hf}$ on p_{O_2}. The process corresponding to R_{lf} showed a $1/R_{lf} \propto p_{O_2}^{\sim 1/2}$ dependence, which indicates that the rate determining step for mass transfer is limited by availability of atomic oxygen [36]. The charge transfer process corresponding to R_{hf} exhibited a $1/R_{hf} \propto p_{O_2}^{\sim 3/8}$ dependence, in agreement with the findings in literature referred to above [33–35,37]. Based on these n values, we suggest an electrode reaction mechanism that involves *i*) dissociative adsorption of oxygen on GDC, *ii*) diffusion of atomic oxygen to the electron transfer sites at the Au/GDC interface, *iii*) first electron charge transfer, and *iv*) second electron transfer, with theoretical dependences of $1/R_p$ on p_{O_2} under given assumptions derived in the literature [33].

$$O_2(g) \leftrightharpoons 2O_{ad(GDC)} \; ; \; i_0 \propto p_{O_2}^1 \quad (i)$$

$$O_{ad(GDC)} \leftrightharpoons O_{ad(Au/GDC)} \; ; \; i_0 \propto p_{O_2}^{1/2} \quad (ii)$$

$$O_{ad(Au/GDC)} + e^- \leftrightharpoons O_{ad(Au/GDC)}^- \; ; \; i_0 \propto p_{O_2}^{3/8} \quad (iii)$$

$$O_{ad(Au/GDC)}^- + e^- + v_o^0 \leftrightharpoons O_{O(GDC)}^{2-} \; ; \; i_0 \propto p_{O_2}^{1/8} \quad (iv)$$

Fig. 5 gives a schematic representation of the ORR mechanism of Au on GDC.

The rate limiting steps are diffusion of atomic oxygen along the two-phase electrode/electrolyte contact followed by the first charge transfer. This is similar to that proposed by Wang and Nowick [34]. While the site for O adsorption whether on GDC or Au was not specified by Wang and Nowick, we suggest oxygen adatom formation on the GDC surface based on the results of the study of the electrode reaction on GDC in O_2+CO_2

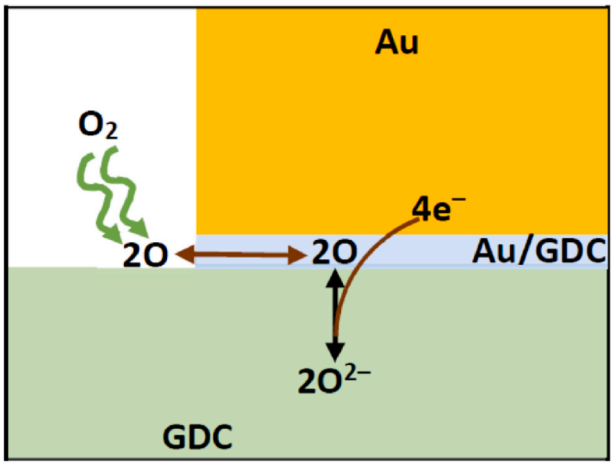

Fig. 5. The electrode reaction of oxygen for Au on GDC.

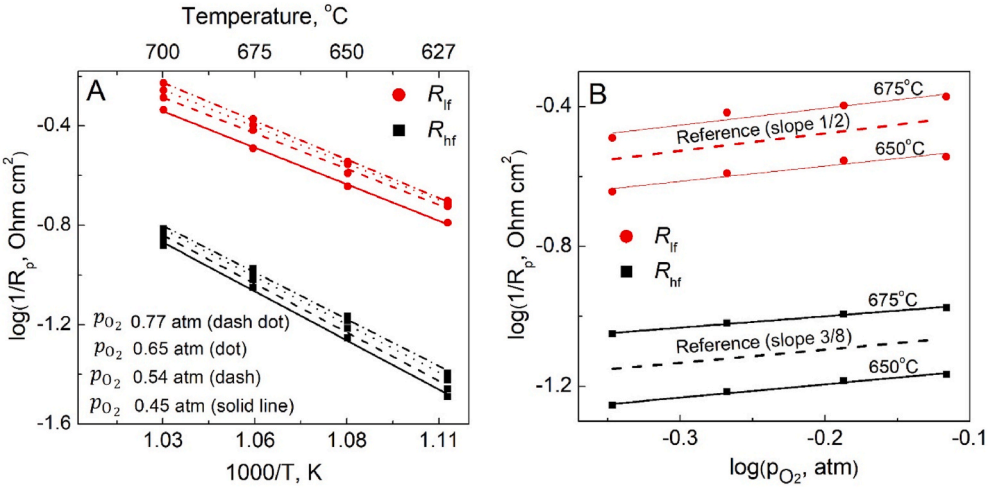

Fig. 4. (A) Arrhenius plot of $1/R_p$ for the rate-limiting electrode reaction processes of Au on GDC under different p_{O_2}; (B) the dependence of $1/R_p$ on p_{O_2} for the electrode reaction process corresponding to R_{lf} and R_{hf} at the Au electrode on the GDC membrane in O_2 atmospheres.

atmospheres (section 3.5).

3.5. Au on GDC in O_2+CO_2 atmosphere

As mentioned above, we experienced considerable adsorption of CO_2 on GDC, depending on p_{CO_2} and temperature. Therefore, the electrode reaction impedances on GDC-based membranes in CO_2-containing atmospheres were hard to interpret as a function of p_{CO_2} or temperature. However, the impedance spectra obtained as a function of p_{O_2} at a fixed p_{CO_2} and temperature were reproducible and allowed us to determine *n*-values from $1/R_p$ versus p_{O_2} plots at a fixed p_{CO_2} at different constant temperatures.

The overall R_p decreased with increasing p_{O_2} at a fixed p_{CO_2} (Fig. 6A). The equivalent circuit model used for the impedance data fitting for O_2 atmospheres, also shown in Fig. 6A, was unsuccessful for O_2+CO_2 atmospheres at temperatures lower than 700 °C, and also other simple circuit models were unsuccessful, possibly due to the blocking effect of the full coverage of adsorbed CO_2. However, the circuit model used for O_2 atmospheres gave good fitting for O_2+CO_2 atmospheres at higher temperatures, giving capacitance values corresponding to CPE1 and CPE2 in the range of 10^{-6} and 10^{-2} F cm^{-2}, respectively.

The $1/R_{lf} \propto p_{O_2}^{\sim 1}$ dependence in O_2+CO_2 atmospheres (Fig. 6B) shows that molecular oxygen is involved in this rate-limiting process, and we conclude that dissociative adsorption of O_2 on GDC (step *i*) is the rds in the first part of the overall reaction: $O_2(g) \rightarrow 2(O_{ad(CTS)})$. The change of rds from step *ii* (O atom diffusion to CTS) in O_2 atmospheres to step *i* (dissociative adsorption of O_2 on GDC) in O_2+CO_2 atmospheres is clearly due to the blockage of O_2 from the GDC surface by the adsorbed CO_2. The higher electrode polarisation resistance on GDC membranes observed in O_2+CO_2 atmospheres than in O_2 atmospheres (Fig. 2) is a direct consequence of the strong, blocking adsorption of CO_2 on GDC. The reaction process corresponding to R_{hf} showed a $1/R_{hf} \propto p_{O_2}^{\sim 3/8}$ dependence (Fig. 6B). It suggests that the second part of the reaction $2(O_{ad(CTS)} + 2e^- + v_o^0 \rightarrow 2O_{o(GDC)}^{2-})$ has a similar rds as in O_2 atmospheres (*i.e.* step *iii*).

3.6. Electrode reaction on the GDC-LNC composite

Section 3.2 showed that the nature of the oxide phase in oxide-carbonate composite membranes influenced the overall R_p in O_2+CO_2 atmospheres; but not in O_2 atmospheres. Consistent with the Raman spectroscopic studies of Chen et al. [20,21], it suggests that CO_4^{2-} having interactions with the oxide phase at the melt-oxide phase interface is the oxygen species in O_2+CO_2 atmospheres [4,18,19]. The experimental identification of *n*-values in CO_2-free O_2 atmospheres was unmanageable due to the chemical decomposition of the carbonate phase [38,39]. The peroxide ions are formed in O_2 atmospheres by the following reaction steps:

$$CO_3^{2-} \leftrightharpoons O^{2-} + CO_2 \quad (4)$$

$$O_2 + 2O^{2-} \leftrightharpoons 2O_2^{2-} \quad (5)$$

Step (4) is the Flood and Førland acid-base self-dissociation equilibrium of carbonate ions. The added CO_2 in gas mixtures shifts this equilibrium towards the carbonate ion side, and reduces the concentration of oxide ions, and hence peroxide formation (reaction (5)) becomes insignificant. The ORR can then only proceed through CO_4^{2-} whose formation, however, is slower than the peroxide formation in CO_2-free O_2 atmospheres. The inhibition of ORR rate on GDC-NLC membranes in O_2+CO_2 atmospheres – and not in CO_2-free O_2 atmospheres – suggests that adsorption of CO_4^{2-}, CO_2, or both CO_4^{2-} and CO_2 with the GDC surface retards the ORR.

Fig. 7 shows the electrode impedance behavior of Au on GDC-LNC

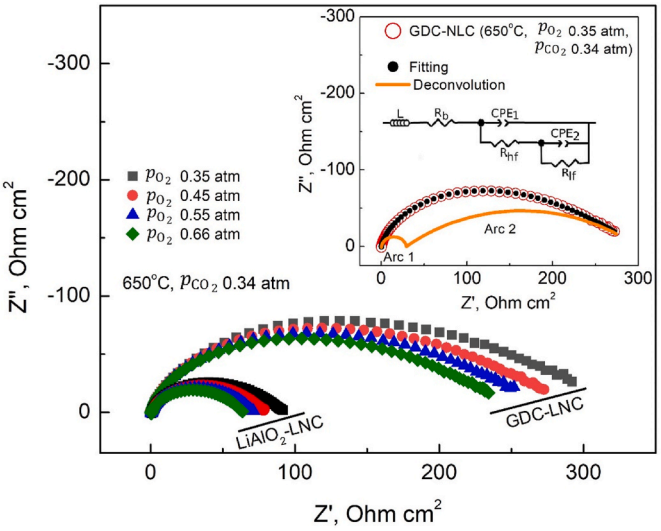

Fig. 7. Complex impedances of electrode polarisation of Au on GDC-LNC and $LiAlO_2$-LNC under O_2+CO_2 atmospheres with different p_{O_2} at a fixed p_{CO_2}. Inset: Equivalent circuit, fitted spectrum, and a deconvolution highlighting the two contributions to the impedance.

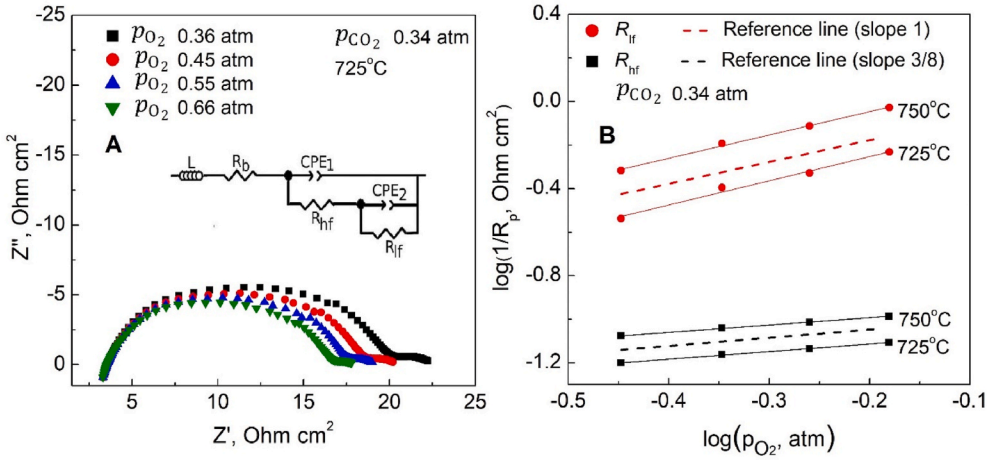

Fig. 6. (A) Complex impedance of the electrode reaction of Au on GDC under O_2+CO_2 atmospheres with different p_{O_2} at a fixed p_{CO_2} (inset: equivalent circuit used for data fitting); (B) the dependence of $1/R_p$ on p_{O_2} for the electrode reaction processes corresponding to R_{lf} and R_{hf} at Au on GDC in O_2+CO_2 atmospheres.

and $LiAlO_2$-LNC membranes in O_2+CO_2 atmospheres as a function of p_{O_2} at a fixed p_{CO_2}. The overall R_p decreased with increasing p_{O_2} for both membranes. Fig. 7 (inset) shows the equivalent circuit used for the impedance data fitting. The characteristic capacitance values corresponding to CPE1 and CPE2 were both in the range 10^{-5} - 10^{-4} F cm^{-2} for Au electrodes on both GDC-LNC and $LiAlO_2$-LNC composite electrolytes. The capacitances are in the range between typical values for charge and mass transfer processes.

There is a significant difference in R_p between Au on GDC-LNC and Au on $LiAlO_2$-LNC. The smaller R_p for $LiAlO_2$-LNC supports the interpretation from above that adsorption of carbonates or CO_2 on GDC impedes the ORR. Fig. 8 shows the dependence of $1/R_{lf}$ and $1/R_{hf}$ on p_{O_2} (fixed p_{CO_2} = 0.34 atm) on GDC-LNC and $LiAlO_2$-LNC at 600 °C. The reaction processes corresponding to R_{hf} and R_{lf} on $LiAlO_2$-LNC exhibited dependences of $1/R_{hf} \propto p_{O_2}^{\sim 1}$ and $1/R_{lf} \propto p_{O_2}^{\sim 1/4}$, respectively, at different temperatures. Based on these *n*-values, we suggest an electrode reaction mechanism that involves *v*) formation of CO_5^{2-} from reaction of O_2 with CO_3^{2-}, *vi*) formation of CO_4^{2-}, *vii*) diffusion of CO_4^{2-} to the first electron transfer site, *viii*) first electron charge transfer, *ix*) transfer of O^- to the second electron transfer site, and *x*) second electron transfer, with theoretical dependences of $1/R_p$ on p_{O_2} as follows:

$$CO^{2-}_{3(LNC)} + O_2(g) \leftrightharpoons CO^{2-}_{5(LNC)}; \quad i_0 \propto p^{1}_{O_2} \tag{v}$$

$$CO^{2-}_{5(LNC)} + CO^{2-}_{3(LNC)} \leftrightharpoons 2CO^{2-}_{4(LNC)}; \quad i_0 \propto p^{1}_{O_2} \tag{vi}$$

$$CO^{2-}_{4(LNC)} \leftrightharpoons CO^{2-}_{4(FETS)}; \quad i_0 \propto p^{1/2}_{O_2} \tag{vii}$$

$$CO^{2-}_{4(FETS)} + e^- \leftrightharpoons CO^{2-}_{3(LNC)} + O^-_{(FETS)}; \quad i_0 \propto p^{3/8}_{O_2} \tag{viii}$$

$$O^-_{(FETS)} \leftrightharpoons O^-_{(SETS)}; \quad i_0 \propto p^{1/4}_{O_2} \tag{ix}$$

$$O^-_{(SETS)} + e^- + CO_2 \leftrightharpoons CO^{2-}_{3(LNC)}; \quad i_0 \propto p^{1/8}_{O_2} \tag{x}$$

The overall reaction for steps (*v*) and (*vi*) is $O_2 + 2CO_3^{2-} = 2CO_4^{2-}$ with *n*-value of 1. The $1/R_{hf} \propto p_{O_2}^{\sim 1}$ dependence shows that this CO_4^{2-} formation process is an rds for the ORR of Au on $LiAlO_2$-LNC membranes [36]. The reaction of the O_2 molecule with CO_3^{2-} (step (*v*)) is an interaction of the lone pair of the oxygen atom of CO_3^{2-} with the π^* antibonding orbital of the O_2 molecule ($[CO_2–O]^{2-}$ + O–O = $[CO_2O–O–O]^{2-}$)[40]. The binding is favourably exothermic at -102 kJ mol^{-1} for $O_2 + 2CO_3^{2-} = 2CO_4^{2-}$, while the CO_4^{2-} formation step (*vi*), which involves an O–O bond breaking and an O–O bond making ($[CO_2O–O–O]^{2-}$ + $[CO_2–O]^{2-} = 2[CO_2O–O–O]^{2-}$) is endothermic [40]. The (first) electron transfer to CO_4^{2-} (step *viii*) is not an rds because the lowest unoccupied molecular orbital (LUMO) which receives electrons has considerably lower energy for CO_4^{2-} than for even O_2^{2-} [40].

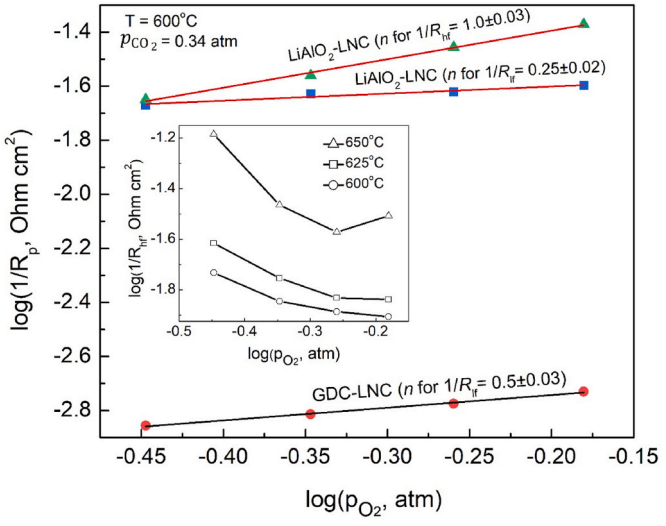

Fig. 8. The dependence of $1/R_p$ on p_{O_2} for the electrode reaction process at Au electrodes corresponding to R_{lf} on GDC-LNC and $LiAlO_2$-LNC membranes, and R_{hf} on $LiAlO_2$-LNC membranes in O_2+CO_2 atmospheres. Inset: The dependence of $1/R_{hf}$ on p_{O_2} for the electrode process at Au electrodes on GDC-LNC membranes at different temperatures in O_2+CO_2 atmospheres.

The $1/R_{lf} \propto p_{O_2}^{\sim 1/4}$ dependence is generally attributed to the transfer of O^- from the first electron transfer site to another site such as a surface step or ledge before the second electron transfer (step (*ix*)) [34,37]. However, voltammetric studies of oxygen reduction on gold electrodes in LNC electrolytes, especially at pressures higher than atmospheric, have shown a reversible spike peak overlapping the oxygen reduction wave [41–43]. The spike peak is due to the redox reaction of adsorbed O^- species on gold electrodes (Au-[O^-]) in O_2+CO_2 atmospheres. It makes us propose a mechanism which does not include the less convincing O^- diffusion to a second electron transfer site. In this case, step (*viii*) changes to

$$CO^{2-}_{4(FETS)} + Au + e^- \leftrightharpoons CO^{2-}_{3(LNC)} + Au - [O^-]; \; i_0 \propto p^{3/8}_{O_2} \tag{viiia}$$

The electrochemical reduction of Au-[O^-] is not feasible at potentials more positive than the spike peak potential, so it follows a reaction path that involves O_2^{2-} formation by O^- association. Therefore, steps (*ix*) and (*x*) change to:

$$Au - [O^-] + Au - [O^-] \leftrightharpoons O_2^{2-} + 2Au; \; i_0 \propto p^{1/4}_{O_2} \tag{ixa}$$

$$O_2^{2-} + Au + e^- + CO_2 \leftrightharpoons CO^{2-}_{3(LNC)} + Au - [O^-]; \; i_0 \propto p^{1/8}_{O_2} \tag{xa}$$

The observed $1/R_{lf} \propto p_{O_2}^{\sim 1/4}$ dependence is therefore attributed to step (*ix a*) for ORR on $LiAlO_2$-LNC membranes.

Fig. 8 shows that R_{lf} makes a dominating contribution to the overall R_p on GDC-LNC membranes. It made the R_p on GDC-LNC membranes higher than that on $LiAlO_2$-LNC membranes or even on GDC membranes. The $1/R_{lf} \propto p_{O_2}^{\sim 1/2}$ dependence shows that the rds corresponding to R_{lf} is oxygen (O) transport (as CO_4^{2-}) to the electron transfer sites (step (*vii*)). Presumably, the GDC of GDC-LNC membranes has adsorbed carbonates ions at oxide ion vacancies and CO_2 at oxide ion sites. The sluggish O transport in GDC-LNC membranes – and not in $LiAlO_2$-LNC membranes – shows that O in CO_4^{2-} has strong interactions with GDC, most likely by the frequent cogwheel type O transfer with adsorbed carbonates at melt-GDC interfaces.

The dependence of $1/R_{hf}$ on p_{O_2} for GDC-LNC membranes did not show linear behavior (Fig. 8 (inset)). Remarkably, $1/R_{hf}$ at lower p_{O_2} values decreased with increasing p_{O_2}. The extent of this negative relation decreased at higher p_{O_2} values, and $1/R_{hf}$ at high pO_2 values started to rise with increasing p_{O_2} at higher temperatures (650 °C). These observations indicate that increasing p_{O_2} changes the rds corresponding to R_{hf} from a process that does not require externally supplied O_2 to an ORR step. Wang and Nowick showed that electrolyte reduction occurs if the surface diffusion rate of O adatom to the interface of Au electrode and doped ceria is slower than the local rate of charge transfer for ORR [34]. Fig. 1B shows that the overall R_p on GDC-NLC membranes in O_2+CO_2 atmospheres is much higher than that on GDC membranes. An extreme case of the diffusion limitation of oxygen species to the charge transfer sites resulted in this higher R_p on GDC-NLC membranes (Fig. 8). Therefore, the electrolyte reduction would be the rds corresponding to R_{hf} under O_2+CO_2 atmospheres containing low p_{O_2}. The high p_{O_2} in O_2+CO_2 atmospheres and high temperatures alleviate the diffusion limitation of oxygen species, and the rds shifts to an ORR step.

4. Conclusions

Electrode reactions at Au on GDC and GDC-LNC membranes were studied by EIS in CO_2/O_2 atmospheres. The diffusion of oxygen adatoms

from the GDC surface to the Au-GDC interface, followed by its reduction to O^- ions, limits the overall ORR rate on GDC membranes in CO_2-free atmospheres. The adsorption of CO_2 on GDC inhibits the rate of oxygen adatom formation on GDC and makes the electrode polarisation resistance on GDC membranes significantly higher in O_2+CO_2 atmospheres than in O_2 atmospheres. The molten carbonate phase of GDC-LNC membranes significantly reduced the electrode polarisation resistance in O_2 atmospheres, but this is attributed to the reaction mechanism going via peroxide formation in the melt rather than the influence of the GDC phase. $LiAlO_2$-LNC membranes showed similar R_p as GDC-LNC in O_2 atmospheres, supporting the independence of the ceramic phase for the peroxide reaction path. In O_2+CO_2 atmospheres, the electrode polarisation resistance on GDC-LNC membranes was significantly higher than that on single-phase GDC and $LiAlO_2$-LNC membranes. The interactions of oxygen species (CO_4^{2-}) with adsorbed carbonates on the GDC phase results in a sluggish transfer of O to the charge transfer sites, giving high R_p and making GDC-LNC membranes less suitable for MCFC applications.

Credit authorship contribution statement

Vijayan Sobhana Dilimon: performed the experimental study, interpreted the results, and wrote the manuscript. **Ragnar Strandbakke:** supervised the experimental study, data collection, and interpretation, and contributed to the writing of the manuscript. **Truls Norby:** conceptualised the research and managed the project, supervised the research, and finalised the manuscript and its revision.

Declaration of competing interest

The authors declare that they have no known competing financial interests or personal relationships that could have appeared to influence the work reported in this paper.

Acknowledgement

The research leading to these results was funded by the MOCO3 project (272688) granted by the Research Council of Norway through the EU M-ERA.NET program.

References

[1] Y. Li, Z. Rui, C. Xia, M. Anderson, Y.S. Lin, Performance of ionic-conducting ceramic/carbonate composite material as solid oxide fuel cell electrolyte and CO_2 permeation membrane, Catal. Today 148 (2009) 303–309.
[2] L. Fan, C. Wang, M. Chen, B. Zhu, Recent development of ceria-based (nano) composite materials for low temperature ceramic fuel cells and electrolyte-free fuel cells, J. Power Sources 234 (2013) 154–174.
[3] A.L. Dicks, Molten carbonate fuel cells, Curr. Opin. Solid State Mater. Sci. 8 (2004) 379–383.
[4] C. Ricca, A. Ringuedé, M. Cassir, C. Adamo, F. Labat, Conduction mechanisms in oxide-carbonate electrolytes for SOFC: highlighting the role of the interface from first-principle modelling, J. Phys. Chem. C 122 (2018) 10067–10077.
[5] L. Fan, C. He, B. Zhu, Role of carbonate phase in ceria–carbonate composite for low temperature solid oxide fuel cells: a review, Int. J. Energy Res. 41 (2017) 465–481.
[6] Y. Zhao, C. Xia, Z. Xu, Y. Li, Validation of H^+/O^{2-} conduction in doped ceria-carbonate composite material using an electrochemical pumping method, Int. J. Hydrogen Energy 37 (2012) 11378–11382.
[7] B. Zhu, Next generation fuel cell R&D, Int. J. Energy Res. 30 (2006) 895–903.
[8] B. Zhu, S. Li, B.-E. Mellander, Theoretical approach on ceria-based two-phase electrolytes for low temperature (300−600 °C) solid oxide fuel cells, Electrochem. Commun. 10 (2008) 302–305.
[9] W. Liu, Y.Y. Liu, B. Li, T.D. Sparks, X. Wei, W. Pan, Ceria (Sm^{3+}, Nd^{3+})/carbonates composite electrolytes with high electrical conductivity at low temperature, Compos. Sci. Technol. 70 (2010) 181–185.
[10] A.I.B. Randão, N.C.T. Martins, S.G. Patrício, F.M.B. Marques, Ionic transport in (nano)composites for fuel cells, Int. J. Hydrogen Energy 41 (2016) 7666–7675.
[11] C.M.C. Soares, S.G. Patrício, F.M.L. Figueiredo, F.M.B. Marques, Relevance of the ceramic content on dual oxide and carbonate-ion transport in composite membranes, Int. J. Hydrogen Energy 39 (2014) 5424–5432.
[12] K. Czelej, K. Cwieka, J.C. Colmenares, K.J. Kurzydlowski, Atomistic insight into the electrode reaction mechanism of the cathode in molten carbonate fuel cells, J. Mater. Chem. 5 (2017) 13763–13768.
[13] K. Czelej, K. Cwieka, J.C. Colmenares, K.J. Kurzydlowski, Catalytic activity of NiO cathode in molten carbonate fuel cells, Appl. Catal., B 222 (2018) 73–75.
[14] Z. Shao, W. Zhou, Z. Zhu, Advanced synthesis of materials for intermediate-temperature solid oxide fuel cells, Prog. Mater. Sci. 57 (2012) 804–874.
[15] B.K. Lee, S.-M. Bae, J.-H. Lee, J. Hwang, Characterization of electrode polarization losses in solid oxide fuel cells: impedance spectroscopy involving spatially-limited electrode geometry, J. Phys. Chem. Solid. 74 (2013) 496–503.
[16] Y. Gong, X. Li, L. Zhang, W. Tharp, C. Qin, K. Huang, Promoting electrocatalytic activity of a composite SOFC cathode $La_{0.8}Sr_{0.2}MnO_{3+\delta}/Ce_{0.8}Gd_{0.2}O_{2-\delta}$ with molten carbonates, J. Electrochem. Soc. 161 (2014) F226–F232.
[17] Y. Gong, X. Li, L. Zhang, W. Tharp, C. Qin, K. Huang, Molten carbonates as an effective oxygen reduction catalyst for 550–650°C solid oxide fuel cells, J. Electrochem. Soc. 160 (2013) F958–F964.
[18] X. Lei, K. Haines, K. Huang, C. Qin, Density functional theory study of oxygen migration in molten carbonate, J. Power Sources 301 (2016) 161–166.
[19] X. Lei, K. Haines, K. Huang, C. Qin, DFT study of oxygen dissociation in molten carbonate, J. Phys. Chem. 119 (2015) 8806–8812.
[20] L.-J. Chen, X. Cheng, C.-J. Lin, C.-M. Huang, In-situ Raman spectroscopic studies on the oxide species in molten Li/K_2CO_3, Electrochim. Acta 47 (2002) 1475–1480.
[21] L.-J. Chen, C.-J. Lin, J. Zuo, L.-C. Song, C.-M. Huang, First spectroscopic observation of peroxocarbonate/peroxodicarbonate in molten carbonate, J. Phys. Chem. B 108 (2004) 7553–7556.
[22] T. Norby, Emf method determination of conductivity contributions from protons and other foreign ions in oxides, Solid State Ionics 28–30 (1988) 1586–1591.
[23] A. Markovits, J. Ahdjoudj, C. Minot, Theoretical study of the adsorption of acids and bases on TiO_2 and MgO surfaces, Il Nuovo Cimento D 19 (1997) 1719–1726.
[24] M. Calatayud, A. Markovits, M. Menetrey, B. Mguig, C. Minot, Adsorption on perfect and reduced surfaces of metal oxides, Catal. Today 85 (2003) 125–143.
[25] K.R. Hahn, M. Iannuzzi, A.P. Seitsonen, J. Hutter, Coverage effect of the CO_2 adsorption mechanisms on CeO_2(111) by first principles analysis, J. Phys. Chem. C 117 (2013) 1701–1711.
[26] T. Jin, Y. Zhou, G.J. Mains, J.M. White, Infrared and X-ray photoelectron spectroscopy study of CO and CO_2 on Pt/CeO_2, J. Phys. Chem. 91 (1987) 5931–5937.
[27] C. Li, Y. Sakata, T. Arai, K. Domen, K. Maruya, T. Onishi, Carbon monoxide and carbon dioxide adsorption on cerium oxide studied by Fourier-transform infrared spectroscopy, J. Chem. Soc. Faraday Trans. I 85 (1989) 929–943.
[28] K. Yoshikawa, H. Sato, M. Kaneeda, J.N. Kondo, Synthesis and analysis of CO_2 adsorbents based on cerium oxide, *J. CO_2 Util.* 8 (2014) 34–38.
[29] K. Yoshikawa, M. Kaneeda, H. Nakamura, Development of novel CeO_2-based CO_2 adsorbent and analysis on its CO_2 adsorption and desorption mechanism, Energy Proc. 114 (2017) 2481–2487.
[30] Z.A. Feng, M.L. Machala, W.C. Chueh, Surface electrochemistry of CO_2 reduction and CO oxidation on Sm-doped CeO_{2-x}: coupling between Ce^{3+} and carbonate adsorbates, Phys. Chem. Chem. Phys. 17 (2015) 12273–12281.
[31] D. Chen, R. Ran, K. Zhang, J. Wang, Z. Shao, Intermediate-temperature electrochemical performance of a polycrystalline $PrBaCo_2O_{5+\delta}$ cathode on samarium-doped ceria electrolyte, J. Power Sources 188 (2009) 96–105.
[32] B.A.V. Hassel, B.A. Boukamp, A.J. Burggraaf, Electrode polarization at the Au, O_2 (g)/yttria stabilized zirconia interface. Part I: theoretical considerations of reaction model, Solid State Ionics 48 (1991) 139–154.
[33] B.A.V. Hassel, H.J.M. Bouwmeester, Electrode properties of Sr-doped $LaMnO_{3}$on yttria-stabilized zirconia. Part II: electrode kinetics, J. Electrochem. Soc. 144 (1997) 134–140.
[34] D.Y. Wang, A.S. Nowick, Diffusion-controlled polarization of Pt, Ag, and Au electrodes with doped ceria electrolyte, J. Electrochem. Soc. 128 (1981) 55–63.
[35] S.P.S. Badwal, H.J. de Bruin, A.D. Franklin, Impedance spectroscopy of the Pt/yttria doped ceria interface, Solid State Ionics 9 10 (1983) 973–978.
[36] Y. Takeda, R. Kanno, M. Noda, Y. Tomida, O. Yamamoto, Cathodic polarization phenomena of perovskite oxide electrodes with stabilized zirconia, J. Electrochem. Soc. 134 (1987) 2656–2661.
[37] J.-D. Kim, G.-D. Kim, J.-W. Moon, Y.-i. Park, W.-H. Lee, K. Kobayashi, M. Nagai, C. E. Kim, Characterization of LSM–YSZ composite electrode by ac impedance spectroscopy, Solid State Ionics 143 (2001) 379–389.
[38] P. Tomczyk, M. Mosiałek, Investigation of the oxygen electrode reaction in basic molten carbonates using electrochemical impedance spectroscopy, Electrochim. Acta 46 (2001) 3023–3032.
[39] M. Cassir, G. Moutiers, J. Devynck, Stability and characterization of oxygen species in alkali molten carbonate: a thermodynamic and electrochemical approach, J. Electrochem. Soc. 140 (1993) 3114–3123.
[40] C. Qin, A. Gladney, DFT study of CO_4^{2-} and CO_5^{2-} relevant to oxygen reduction with the presence of molten carbonate in solid oxide fuel cells, Comput. Theor. Chem. 999 (2012) 179–183.
[41] C.-G. Lee, K. Yamada, T. Nishina, I. Uchida, A kinetic study of spike peaks observed under pressurized oxidant gas atmospheres in molten alkali carbonates, J. Electrochem. Soc. 143 (1996) 2315–2318.
[42] B.B. Davé, R.E. White, S. Srinivasan, A.J. Appleby, Electrode kinetics of oxygen reduction in lithium carbonate melt: use of impedance analysis and cyclic voltammetric techniques to determine the effects of partial pressure of oxygen, J. Electrochem. Soc. 138 (1991) 673–678.
[43] M. Mohamedi, Y. Hisamitsu, Y. Ono, T. Itoh, I. Uchida, Influence of adsorption phenomena upon the mechanism and kinetics of oxygen reduction at a gold electrode in (Li-Na)CO_3 melt, J. Electrochem. Soc. 147 (2000) 490–495.